Design of Wideband In-Phase and Out-of-Phase Power Dividers Using Microstrip-to-Slotline Transitions and Slotline Resonators

He Zhu, *Member, IEEE*, Zhiqun Cheng, and Y. Jay Guo, *Fellow, IEEE*

Abstract—A new class of in-phase and out-of-phase power dividers with constant equal-ripple frequency response and wide operating bandwidth is presented in this paper. The proposed design is based on microstrip-to-slotline transitions and slotline resonators. A slotted T-junction is adopted to split the power into two parts and obtain wideband isolation between the two output signals at the same time. The characteristic impedance of the transitions and resonators determines the operating bandwidth and in-band magnitude response. By reversing the placement direction of the slotline-to-microstrip transition, the electrical field is reversed, thus resulting in out-of-phase responses between output ports. Thorough analysis of the relations between the structure and the characteristic functions are provided to guide the selection of parameters of the structure in order to meet the design objectives. In the structure, Simulation and measurement are conducted to verify the design method. For both in-phase and out-of-phase cases, more than 110% bandwidth has been achieved with excellent matching at all ports and isolation of output signals. Constant in-band ripple is obtained within the operating band of the power dividers, indicating that the proposed design can realise minimal power deviations, which is extremely desired in wireless systems.

Index Terms—In-phase, microstrip-to-slotline transitions, out-of-phase, planar, power divider, slotline resonators, wideband.

I. INTRODUCTION

POWER dividers are crucial microwave components, which have been widely used in various parts of wireless communication systems, such as RF front-ends, feeding networks for antenna arrays, power amplifiers, mixers and reflectometers. To increase the capacity of wireless systems, a wide bandwidth is typically required, thus resulting in high demand of wideband power dividers. To achieve wideband or even ultra-wideband performance, many techniques have been proposed, such as stepped-impedance open-circuit stubs [1], short-circuit stubs [2], slotline resonator [3], broadside coupled structure [4], three-line coupled-line [5] and dual-resonant -mode impedance transformer [6]. Modified structures of the Gysel power divider were illustrated in [7] and [8], where a wideband operating bandwidth was obtained with high power dissipating capability. In a RF front-end, power dividers are
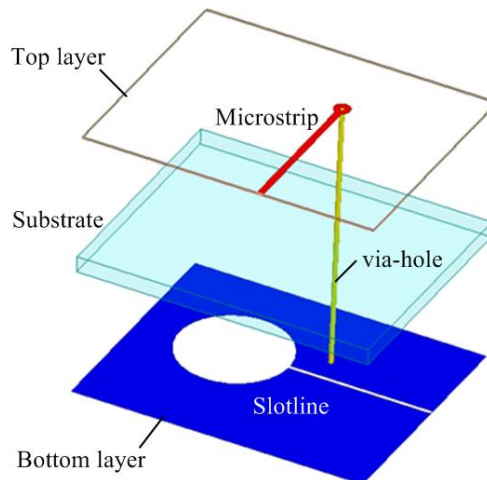
Fig. 1. Layout of the microstrip-to-slotline transition.

usually cascaded with bandpass filters to get rid of undesired signals. Since the cascading devices leads to bulky overall circuit and large losses, it is desirable to include filtering function in power dividers [9]-[15]. Nevertheless, a wide operating bandwidth is always a crucial target in the development of power dividers.

For wideband power dividers, there are two main issues to be focused on: magnitude and phase responses. For the phase response, in-phase [1]-[8], [16]-[18] and out-of-phase [19]-[23] states are the most useful types in microwave systems. To achieve 180° phase difference at two output ports, double-sided parallel striplines [19], substrate-integrated waveguide [20], slotlines [21], [22], and hybrid structure [23] were used. Regarding magnitude response, equal in-band ripple levels are extremely important and demanded to ensure that the magnitude frequency response of the output signals can be highly balanced over a wide operating bandwidth. Therefore, equal in-band ripple level responses were investigated and widely used in various microwave devices like filters [24]-[26], couplers [27], [28], baluns [29], phase shifters [30], impedance transformers [31], [32], etc. In [24], parallel-coupled lines with Chebyshev passbands were synthesized based on the insertion-loss functions. With the specification of the cut-off frequencies and ripple-levels, specific in-band equal-ripple responses can be realised. Since the microstrip-to-slotline transitions are able to provide strong coupling between the
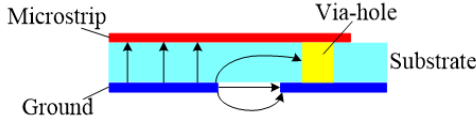
Fig. 2. Electrical-field distribution of the microstrip-to-slotline transition (right-side view).
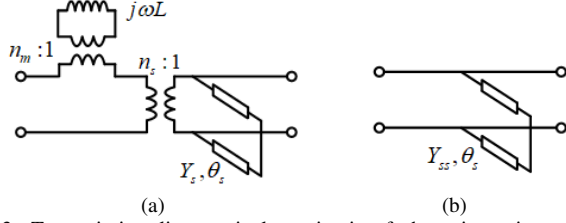

(a)   (b)

Fig. 3. Transmission line equivalent circuit of the microstrip-to-slotline transition (a) original model; (b) simplified model.
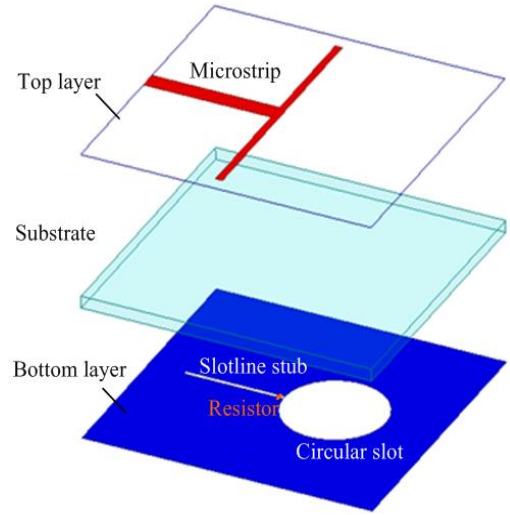
microstrip lines and the slotlines, they are extremely attractive in wideband wireless applications [33]-[35]. This kind of structure can realize equal-ripple in-band magnitude responses, so the slotline resonator and the synthesis approach were widely investigated and used in designing various microwave components and devices. Although equal-ripple response is a very attractive feature and realized in many microwave devices, to our best knowledge, however, no wideband power dividers with in-band equal-ripple responses has been reported.

In this paper, a new class of in-phase and out-of-phase power dividers with constant equal-ripple in-band response and wide isolation band is proposed. The proposed design has achieved the following distinctive features: (1) wideband and constant equal-ripple frequency response is achieved and the in-band ripple-level can be easily controlled; (2) a new structure composed of microstrip-to-slotline transitions and multi-mode slotline resonators is proposed to realize the wide operating bandwidth; (3) in-phase and out-of-phase responses are realized without affecting the magnitude response using the same structure; (4) thorough synthesis and analysis are given to show how to control the bandwidth and ripple-level using the proposed structure; (5) wideband isolation is achieved using a slotted T-junction, which guarantees more than 100% operating bandwidth. Two design prototypes of the wideband power divider with in-phase and out-of-phase response are constructed and simulated in the EM environment. Finally, the synthesis approach and the simulated results are verified successfully by experiments.

II. MICROSTRIP-TO-SLOTLINE TRANSITIONS AND SLOTTED T-JUNCTIONS

A. Microstrip-to-Slotline Transition

Fig. 1 depicts the configuration of the microstrip-to-slotline transition using a short-circuit via-hole. On the ground plane, a slotline is positioned perpendicularly to the microstrip line on top with a short-ended circular slot at one end with radius R_s. The coupling occurs between the microstrip line and the slotline by means of the magnetic field [36]. The circular slot can be regarded as a short-end stub with uniform impedance and a certain amount of electrical length. Its impedance can be

Fig. 4. Layout of the slotted microstrip T-junction.

roughly calculated using the integration method on the circular slot, and the equivalent electrical length was found to be $l_s = 0.75\ R_s$ [37], [38]. Fig. 2 shows the electric-field distribution at the transition position between the microstrip and slotline. The metal via-hole serves as an electric wall to localise the field within the substrate and convert the electrical field in the vertical direction on the microstrip to the horizontal direction in the slotline, thus providing the coupling between the microstrip and the slotline in the ground. Although the via-hole can be replaced by a quarter-wavelength or an open-circuit circular microstrip stub as used in [24]-[26] and [33]-[35], the via-hole is more favoured in achieving bandwidth improvement and the flatness of in-band ripple response.

The microstrip-to-slotline transition can be modelled using a series inductive load L and a parallel short-circuit stub with electrical length of θ_s and characteristic impedance of Z_s [39], [40]. Due to the existing discontinuity of the slot and mutual coupling between the slotline and the microstrip, a transformer with turn ratio of n_s is required, as shown in Fig. 3(a). The parallel short-circuit stub and the cascaded transformer can be simplified using a short-circuit stub with the same electrical length and characteristic impedance of Z_{ss} of $n_s^2 \times Z_s$ (in terms of admittance $Y_{ss} = Y_s/n_s^2$). Besides, since the inductance of L is so small and thus can be neglected, the equivalent circuit of the transition can be modified as shown in Fig. 3(b). In this case, the transition can be simplified as a shunted short-ended stub with electrical length of θ_s and characteristic impedance of Z_{ss}. This structure is very simple and suitable designing wideband microwave components.

B. Slotted Microstrip T-junction

For wideband power dividers, it is challenging to maintain excellent isolation across a wide band. Efforts have been made to increase the isolation bandwidth of power dividers as illustrated in [41], [42]. The typical method is to include lump-elements in circuits like series RC, series RCL or parallel RCL isolation networks [43]-[45]; however, these techniques are not applicable to designing wideband power dividers, since
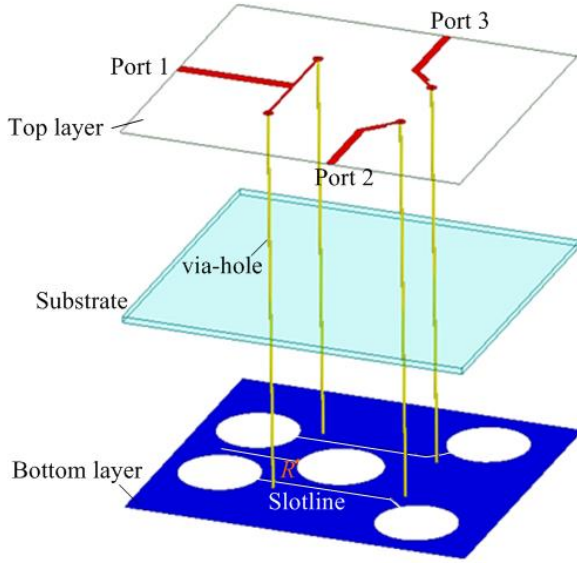
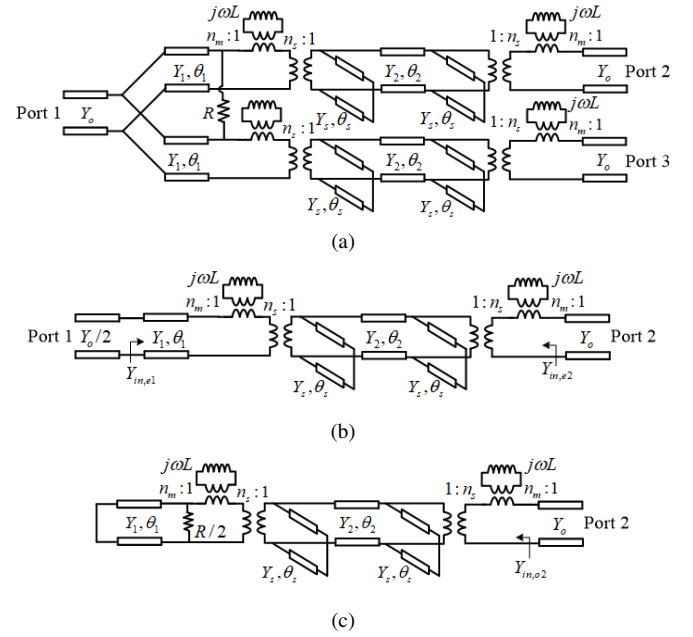Fig. 5. Layout of the proposed wideband in-phase power divider.

Fig. 6. (a) Transmission line equivalent circuit of the proposed power divider; (b) even-mode equivalent circuit; and (c) odd-mode equivalent circuit.

they are frequency-dependent and cannot perform well across such wide bandwidth.

To tackle the problem, a kind of slotted microstrip T-junction with loaded resistor is introduced for designing wideband power dividers, as shown in Fig. 4. Compared with the traditional microstrip T-junction, the proposed structure includes a narrow slotline stub and a circular slot on the ground. The circular slot with radius of R_s is connected with the narrow slot line at the centre of the T-junction, which is located just underneath the microstrip T-junction. The structure was initially used in de Ronde's coupler to achieve high isolation of a coupler [46] because it prevents the current from one arm of the T-junction flowing to the other one, which greatly increases the isolation between two arms. Since the slotline is frequency-independent, this slotted microstrip T-junction can work properly across a wide frequency range providing high isolation. Due to this reason, it is adopted here for isolation improvement of the power divider. Moreover, to further increase the isolation between two arms of the T-junction, a chip resistor is loaded across the slot at the position of the connecting point of the circular slot and the slotline stub. The resistor can absorb the power transfer of the T-junction from one arm to another. As a result, the isolation between two arms of the T-junction has been increased dramatically thus achieving wideband isolation. This kind of structure can effectively increase the isolation between output ports within a power divider, which will be introduced in the next section.

III. ANALYSIS OF THE WIDEBAND POWER DIVIDER

Based on the techniques presented above, a wideband power divider using microstrip-to-slotline transitions with via-holes and slotline resonators is shown in Fig. 5. Two microstrip-to-slotline transitions are shunted with the slotted microstrip T-junction at the input port, and another two transitions are connected in series with two output ports. On the backside of the substrate, two slotlines working as multi-mode

resonators are connected between two microstrip-to-slotline transitions. An isolating resistor is loaded on the ground plane across the slotline stub underneath the microstrip lines. The design is aimed at obtaining wideband equal power division (3-dB) with constant in-band equal-ripple and in-phase frequency response.

Using the equivalent circuit displayed in Fig. 3(a), the wideband power divider can be treated as a three-port network using equivalent transmission-line model shown in Fig. 6(a). Due to the symmetricity of the structure, it can be analysed using even/odd-mode decomposition technique. Fig. 6(b) and (c) show the even- and odd-mode equivalent transmission-line circuit when the even- and odd-mode excitations are applied. Similar to the microstrip-to-slotline transition, in order to have a simple and concise synthesis procedure, the cascaded transformers and paralleled inductors can be regarded as short-circuit and the paralleled transformer can be merged into the shunt stub with a modified value. Therefore, the even- and odd-mode circuit can be simplified as shown in Fig. 7.

On the other hand, the S-parameters of a power divider can be expressed by:

$$S_{11} = S_{11e} \tag{1}$$

$$S_{21} = S_{31} = \frac{S_{21e}}{\sqrt{2}} \tag{2}$$

$$S_{22} = S_{33} = \frac{S_{22e} + S_{22o}}{2} \tag{3}$$

$$S_{32} = \frac{S_{22e} - S_{22o}}{2} \tag{4}$$

For a power divider, the following equations should be satisfied: $|S_{11}| = |S_{22}| = |S_{33}| = 0$, $|S_{21}| = |S_{31}| = 1/\sqrt{2}$, and $|S_{32}| = 0$. These equations ensure perfect matching at all three ports and perfect isolation between output ports. For the transmitted signals, equal power and identical phase should be obtained at two output ports. In the following parts of this
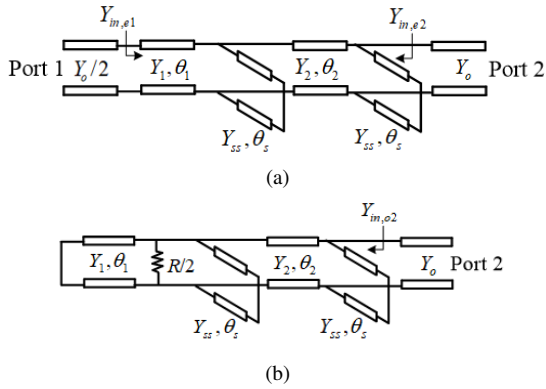
(a)

(b)

Fig. 7. Simplified transmission line equivalent circuit: (a) even-mode; (b) odd-mode.

section, the matching and isolation as well as the wideband response with constant in-band ripple level will be discussed.

A. Matching and Isolation

In Fig. 7(a), the even-mode excitation is applied, which means the central symmetrical plane can be seen as a perfect magnetic wall. In this case, the input port impedance is doubled as $2Z_o$. From (1) it is seen that the matching at the input port is only related to the S_{11} of the even-mode circuit. Therefore, to get perfect matching at all three ports, it is required to get perfect matching at port 1 and port 2 for the even-mode circuit, in other words,

$$Y_{in,e1} = Y_o/2, \text{ and } Y_{in,e2} = Y_o \qquad (5)$$

From Fig. 6(c), it can be found that

$$Y_{in,e1} = Y_1 \frac{Y'_{e1} + jY_1 \tan\theta_1}{Y_1 + jY'_{e1} \tan\theta_1} \qquad (6)$$

$$Y_{in,e2} = Y_2 \frac{Y'_{e2} + jY_2 \tan\theta_2}{Y_2 + jY'_{e2} \tan\theta_2} - jY_{ss} \cot\theta_s \qquad (7)$$

where

$$Y'_{e1} = Y_2 \frac{Y'_e + jY_2 \tan\theta_2}{Y_2 + jY'_e \tan\theta_2} - jY_{ss} \cot\theta_s \qquad (8)$$

$$Y'_e = Y_o - jY_{ss} \cot\theta_s \qquad (9)$$

$$Y'_{e2} = Y_1 \frac{Y_o/2 + jY_1 \tan\theta_1}{Y_1 + jY'_{e1} \tan\theta_1/2} - jY_{ss} \cot\theta_s \qquad (10)$$

As mentioned above, the electrical length of the shunted stubs is quarter-wavelength at the center frequency f_o. Since the slotline would work as a multi-mode resonator, the electrical length of the slotline is chosen as half-wavelength at f_o. Besides, θ_1 is selected as quarter-wavelength to make port 1 virtual short-circuit seen from the slotline resonator. In a nutshell, the related electrical lengths for all the transmission lines are: $\theta_1 = 90°$, $\theta_2 = 180°$ and $\theta_s = 90°$. Combining (5)-(10), one can find that Y_1 affects the matching of all ports, while Y_2 and Y_{ss} have no effect on the even-mode circuit at f_o. To get perfect matching at f_o, Y_1 should be selected $Y_o/\sqrt{2}$, such as in classic Wilkinson designs; however, for wideband power dividers, this value may vary to some extent.

When the odd-mode excitation is applied as shown in Fig. 7(b), the symmetrical plane can be regarded as virtual electrical wall, which makes port 1 become short-circuit to the ground.
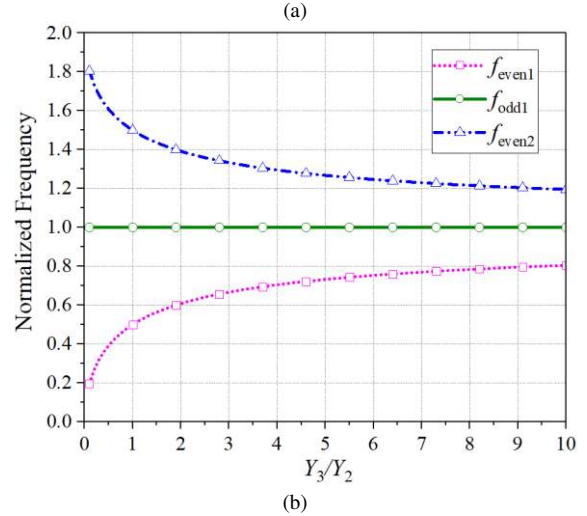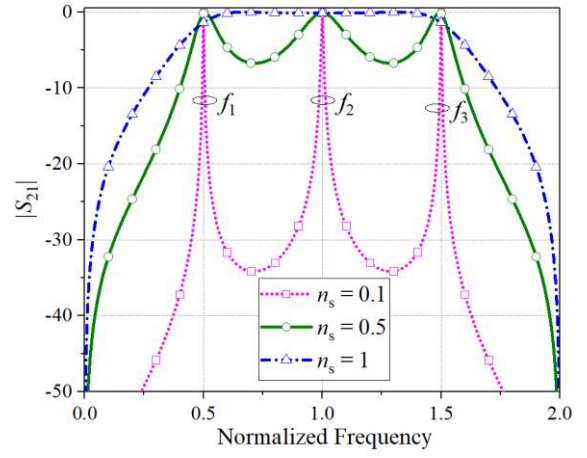

(a)

(b)

Fig. 8. (a) |S$_{21}$| of the power divider with different n_s; (b) resonance distribution against Y_3/Y_2.

As indicated in (3) the matching properties at port 2 and port 3 are related to both of the even-mode and odd-mode circuits. Meanwhile, since the isolation resistor only exists in the odd-mode circuit, the matching of odd-mode circuit is also related to the isolation performance of the power divider, which requires that $Z_{in,o2} = Z_o$. From Fig. 7(b), it can be calculated that

$$Y_{in,o2} = Y_2 \frac{Y'_o + jY_2 \tan\theta_2}{Y_2 + jY'_o \tan\theta_2} - jY_{ss} \cot\theta_s \qquad (11)$$

where

$$Y'_o = -jY_{ss} \cot\theta_s + Y_1 \frac{2/R + jY_1 \tan\theta_1}{Y_1 + j \, 2/R \tan\theta_1} \qquad (12)$$

By solving $Y_{in,o2} = Y_o$, the value of the isolating resistor can be determined as $R = 2Y_o/Y_1^2$, which guarantees a perfect matching at port 2 and 3 at f_o. In summary, to get perfect matching at all three ports and perfect isolation between port 2 and port 3, the electrical length should be $\theta_1 = 90°$, $\theta_2 = 180°$ and $\theta_s = 90°$, and the isolating resistor R is selected as $2Z_o$. The admittance of Y_1 is related to both of matching and transmission characteristics, which should be taken into consideration at the same time. The admittances of Y_2 and Y_{ss}, though have no effect on the matching and isolation of the power divider, will affect the resonance as well as the in-band
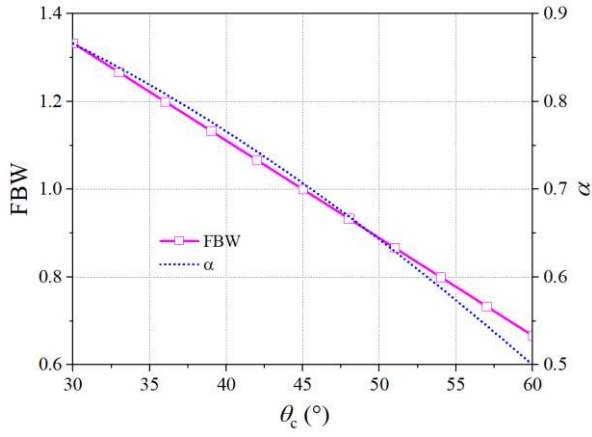
Fig. 9. Relation between θ_c and FBW/α.

magnitude response of the power dividers, which will be discussed in the next section.

B. Resonances

In this design, slotline resonators are used as multi-mode resonators to realize wideband performance. The slotline resonator is described as a transmission line (Y_2, θ_2) with uniform admittance as well as two short-ended stubs (Y_{ss}, θ_3) in Fig. 7. The lengths of θ_2 and θ_3 are fixed at half-wavelength and quarter-wavelength at the center frequency, respectively. As indicated in (1b), the power transmission is only related to the even-mode circuit, which is depicted in Fig. 6(b). In this design, since the slotline works as a three-mode resonator, when the resonator is weakly coupled ($n_s = 0.1$), the three resonator poles can be easily observed. A wideband and constant passband can be obtained by increasing the coupling. When $n_s = 0.1$, a flat and constant magnitude can be realized. Since the resonator is symmetric, it is possible to find the positions of all the resonances by calculating its odd-mode and even-mode resonances, respectively. For the odd-mode resonance θ_{odd}, o

$$Y_{odd} = j\frac{Y_2}{\tan(\theta_{odd})} = 0 \tag{13}$$

and thus,

$$\theta_{odd} = \tan^{-1}\infty = \left(\frac{1}{2} + n\right)\pi \tag{14}$$

For the even-mode case, the slotline resonator operates as a half-wavelength stepped-impedance resonator. The input impedance of the resonator can be written as:

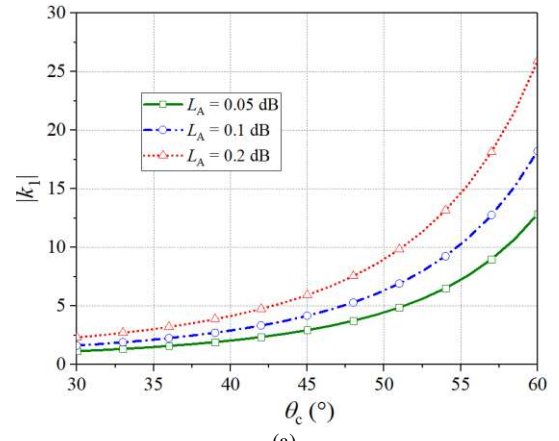$$Y_{even} = jY_2\frac{Y_2\tan\theta_2\tan\theta_3 - Y_3}{Y_2\tan\theta_3 + Y_3\tan\theta_2} \tag{15}$$

To find the even-mode resonances, one has $Y_{even} = 0$, which leads to $Y_2\tan^2\theta_{even} - Y_3 = 0$. The positions of two even-mode resonances are thus given by:

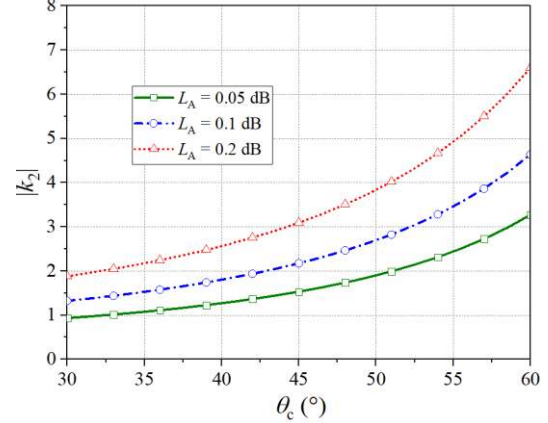$$\theta_{even1} = \tan^{-1}\sqrt{Y_3/Y_2} + n\pi \tag{16}$$

$$\theta_{even2} = \pi - \tan^{-1}\sqrt{Y_3/Y_2} + n\pi. \tag{17}$$

Since the centre frequency f_o is located at $\pi/2$, the three modes of the slotline resonator are located at the following positions:

$$f_{even1} = \frac{2f_o}{\pi}\tan^{-1}\sqrt{Y_3/Y_2} \tag{18}$$

(a)

(b)

Fig. 10. Relations between function coefficients and θ_c when L_A is 0.05 dB, 0.1 dB and 0.2 dB: (a) $|k_1|$ and (b) $|k_2|$.

$$f_{odd1} = f_o \tag{19}$$

$$f_{even2} = \frac{2f_o}{\pi}(\pi - \tan^{-1}\sqrt{Y_3/Y_2}) \tag{20}$$

It is found from (18)-(20) that, the odd-mode resonance is fixed at f_o while two even-mode resonances vary with the admittance ratio of Y_3 and Y_2. The resonance distribution is plotted in Fig. 8. When the ratio of Y_3/Y_2 increases, the first and third mode will move closer to the center frequency, which may result in a smaller bandwidth of the passband. To meet the bandwidth requirement, it is necessary to select an appropriate admittance ratio Y_3/Y_2 during the design process. The selection of resonances is also determined by the objectives of bandwidth and in-band ripple levels, which will be discussed next.

C. In-band Magnitude Response

As mentioned before, for a wideband power divider, it is required that $|S_{21}| = |S_{31}| = 1/\sqrt{2}$. However, for wideband applications, it is practical to make the output response the same for every single frequency. To minimize the difference within the band, it is favorable to have equal in-band ripple level. Therefore, it is possible to predict the in-band performance of the power divider by investigating S_{21e}. To calculate the S-parameters of the two-port network, the ABCD-matrix of the whole circuit can be considered by multiplying the cascaded ABCD-matrix of each part of the circuit:
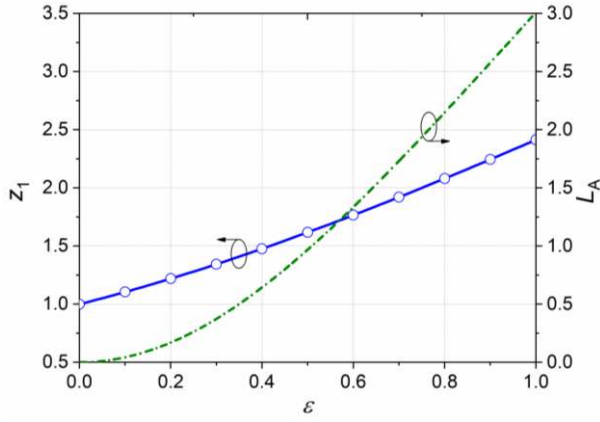
Fig. 11. Value of z_1 and L_A against ε.

$$\begin{bmatrix} A & B \\ C & D \end{bmatrix}_e = M_1 M_s M_2 M_s$$

$$= \begin{bmatrix} \cos\theta_1 & \dfrac{j\sin\theta_1}{y_1} \\ jy_1\sin\theta_1 & \cos\theta_1 \end{bmatrix} \cdot \begin{bmatrix} 1 & 0 \\ -jy_{ss}\cot\theta_s & 1 \end{bmatrix}$$

$$\cdot \begin{bmatrix} \cos\theta_2 & \dfrac{j\sin\theta_2}{y_2} \\ jy_2\sin\theta_2 & \cos\theta_2 \end{bmatrix} \cdot \begin{bmatrix} 1 & 0 \\ -jy_{ss}\cot\theta_s & 1 \end{bmatrix} \quad (21)$$

The electrical lengths of θ_1, θ_2 and θ_s are simplified as $\theta_1 = \theta_s = \theta_2/2 = \theta$. Meanwhile, the squared magnitude of the scattering parameters can be expressed by

$$|S_{21e}|^2 = \frac{1}{1+|F_m|^2}, \quad |S_{11e}|^2 = \frac{|F_m|^2}{1+|F_m|^2} \quad (22)$$

where

$$F_m = \frac{B-C}{2}$$

$$B = -j\left[\left(1+\frac{y_{ss}}{y_1}\right)\cdot\frac{2}{y_2}+\frac{1}{y_1}\right]\cdot\frac{\cos^4\theta}{\sin\theta}$$

$$+j\left[\left(1+\frac{y_{ss}}{y_1}\right)\cdot\frac{2}{y_2}+\frac{3}{y_1}\right]\frac{\cos^2\theta}{\sin\theta}-j\frac{1}{y_1\sin\theta}$$

$$C = -j\left[\left(1+\frac{y_{ss}}{y_2}\right)y_1+y_2+\left(2+\frac{y_{ss}}{y_2}\right)y_{ss}\right]\cdot\frac{\cos^4\theta}{\sin\theta}$$

$$+j\left[2\left(1+\frac{y_{ss}}{y_2}\right)y_1+y_1+2y_2+2y_{ss}\right]\cdot\frac{\cos^2\theta}{\sin\theta}+jy_1\frac{1}{\sin\theta}$$

Therefore, F_m can be expressed as:

$$F_m = j\frac{1}{\sin\theta}(k_1\cos^4\theta + k_2\cos^2\theta + k_3) \quad (23)$$

where

$$k_1 = (y_1+y_{ss})\left(1+\frac{y_{ss}}{y_2}\right)+y_2+y_{ss}-\left(1+\frac{y_{ss}}{y_1}\right)\cdot\frac{1}{y_2}+\frac{1}{2y_1} \quad (24)$$

$$k_2 = \left(1+\frac{y_{ss}}{y_1}\right)\cdot\frac{1}{y_2}+\frac{3}{2y_1}-\left(1+\frac{y_{ss}}{y_2}\right)\cdot y_1-\frac{y_1}{2}-y_2-y_{ss} \quad (25)$$

$$k_3 = \frac{1}{2}\left(\frac{1}{y_1}-y_1\right) \quad (26)$$

In order to achieve equal in-band ripple level, it is possible to use a polynomial of $\varepsilon\cos(n\phi+q\xi)$ to replace F_m and write the squared magnitude of S_{21e} as:

$$|S_{21e}|^2 = \frac{1}{1+\varepsilon^2\cos^2(n\phi+q\xi)}$$

$$= \frac{1}{1+\varepsilon^2[T_n(x)T_q(y)-U_n(x)U_q(y)]} \quad (27)$$

where ε is ripple constant which is related to the specified in-band ripple level; $T_n(x)$ and $U_n(x)$ are the Chebyshev polynomial functions of the first and second kinds of degree n. The coefficients of n and q are required to be fixed as 1 and 3. To describe the bandwidth of the passband, it is possible to define a variable $\alpha = 1/\cos\theta_c$, where θ_c is the lower cut-off frequency of the passband. Correspondingly, the higher cut-off frequency is $(180°-\theta_c)$, the fractional bandwidth of the passband is $(180°-2\theta_c)/90°$, and

$$\cos\phi = \alpha\cos\theta \quad (28)$$

$$\cos\xi = \cos\phi\sqrt{\frac{\alpha^2-1}{\alpha^2-\cos^2\phi}} \quad (29)$$

Fig. 9 shows the relation between θ_c and FBW as well as α. The value of θ_c determines the FBW and α, which affects the impedance of the structure. Based on the aforementioned relations, the item of $\varepsilon\cos(n\phi+q\xi)$ can be written as

$$\varepsilon\cos(n\phi+q\xi) = j\frac{1}{\sin\theta}\left[-\varepsilon\left(4\alpha^2+4\alpha^3\sqrt{\alpha^2-1}\right)\cos^4\theta\right.$$
$$\left.-\varepsilon\left(5\alpha^2+3\alpha\sqrt{\alpha^2-1}\right)\cos^2\theta+\varepsilon\right] \quad (30)$$

Comparing (24) with (17), the functions coefficients of k_1, k_2 and k_3 can be expressed as

$$k_1 = -\varepsilon\left(4\alpha^2+4\alpha^3\sqrt{\alpha^2-1}\right) \quad (31)$$

$$k_2 = -\varepsilon\left(5\alpha^2+3\alpha\sqrt{\alpha^2-1}\right) \quad (32)$$

$$k_3 = \varepsilon \quad (33)$$

By equating (24)-(26) with (31)-(33), the related parameters of y_1, y_2 and y_{ss} can be determined with specific given value of ε and α. Since the bandwidth of the passband and in-band ripple level are related to ε and α, it is possible to obtain a desired bandwidth and in-band ripple level by selecting appropriate value of y_1, y_2 and y_{ss}. With different selections of ε and α, the function coefficients of k_1, k_2 and k_3 are also different. The ripple level L_A is related to the ripple constant by $\varepsilon = \sqrt{10^{L_A/10}-1}$. When the in-band ripple level is given, the values of to ε and α are fixed, which means that k_1, k_2 and k_3 can be determined using (31)-(33). Then, the related value of admittances y_1, y_2 and y_{ss} can be solved from (24)-(26). Since α is related to θ_c and ε is related to L_A, the relations between k_1, k_2 and θ_c are shown in Figs. 10(a) and (b), where L_A is selected as 0.05 dB, 0.1 dB and 0.2 dB, respectively. Apparently, both of k_1 and k_2 are negative, and the absolute value of k_1 and k_2 will increase when a larger value of L_A or θ_c is selected.
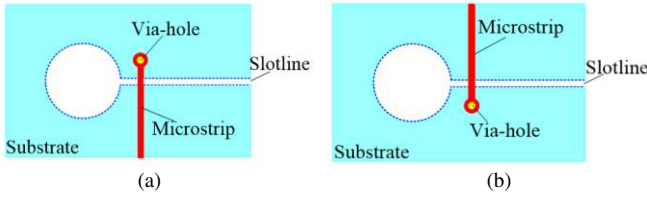
Fig. 12. Two different configurations of slotline-to-microstrip transitions (Top view): (a) original placement; (b) Reversed placement.
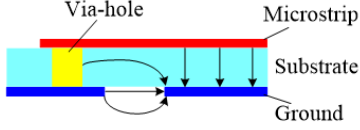

Fig. 13. Electrical-field distribution of the slotline-to-microstrip transition when the via-hole is reversely placed (right-side view).
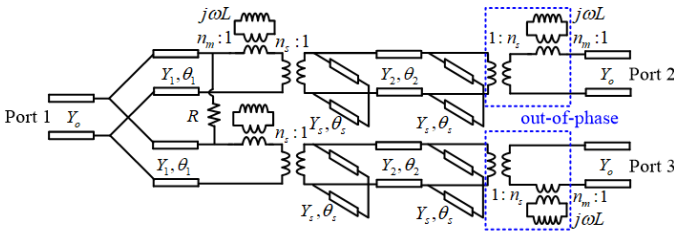

Fig. 14. Equivalent circuit of the proposed wideband power divider with out-of-phase response.

On the other hand, by observing (26) and (32) one can find that the ripple constant ε determines the value of the admittance of y_1. Therefore, when the value of ε is determined, the impedance of z_1 can be calculated by

$$\varepsilon = \sqrt{\frac{z_1^2 - 1}{2z_1}} \tag{34}$$

$$z_1 = \varepsilon + \sqrt{\varepsilon^2 + 1} \tag{35}$$

Fig. 11 shows the relation between ε and L_A as well as z_1. The value of ε will drop when a smaller value of L_A is used. It is seen from (35) that z_1 is always larger than 1, and z_1 will be larger when ε increases. In this design, the target of an example prototype is set as $L_A = 0.1$ dB, which means $\varepsilon = 0.1526$. In this case, z_1 should be chosen as 58.2 Ω. When z_1 is found, equations (24) and (25) are reduced to two quadric equations with two variables y_2 and y_{ss}, which are very easy to solve. The value of y_2 is the admittance of the slotline resonator, while the admittance of the short-circuit slot stub y_s can be found using $y_s = n_s^2 \cdot y_{ss}$. The turn ratio value n_s is also related to the ripple level and bandwidth; a larger n_s will lead to a wider bandwidth.

IV. SYNTHESIS OF WIDEBAND IN-PHASE AND OUT-OF-PHASE POWER DIVIDERS

A. In-phase and Out-of-phase Responses

The aforementioned analysis has demonstrated that the proposed structure can realize constant ripple level frequency response regarding to the magnitude of output signals. In regards to the phase response, since the proposed structure
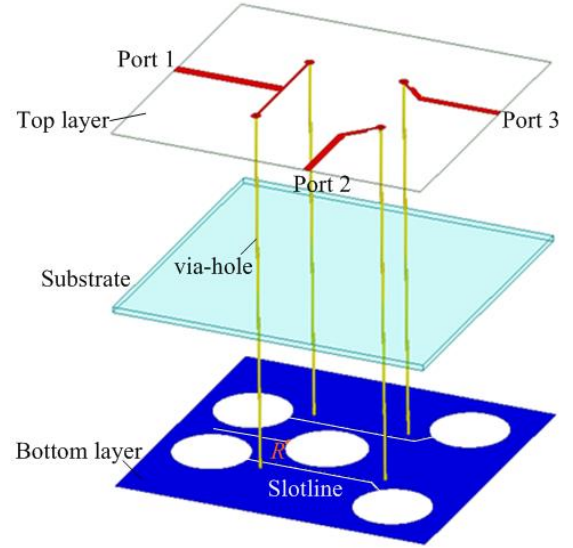

Fig. 15. Layout of the proposed power divider with out-of-phase response.

shown in Fig. 5 is fully symmetrical, the phase and magnitude responses are identical as well. However, in some cases, the out-of-phase response is also required, which means the output signals should have the same frequency response in magnitude while having opposite signs in phase.

In this work, it is possible to realize out-of-phase response using different configurations of slotline-to-microstrip transitions, as illustrated in Fig. 12. In Fig. 10(a), it is assumed that the signal is propagating in the slotline with the same electrical-field distribution compare with Fig. 2. In this case, the electrical-field in the microstrip will have the same amount of field lines and the same direction as displayed in Fig. 2. If the position of the via-hole and the microstrip line are reversely placed at the opposite side across the slotline, as indicated in Fig. 12(b), the direction of electric-field lines will be reversed. As indicated in Fig. 13, the produced electrical-field will have the same amount of field lines compared with the original method of placement shown in Fig. 12(a), indicating that the phase responses of two cases are opposite while the magnitude is the same. Therefore, it is possible to apply these two types of transitions to different signal paths in the design of out-of-phase power dividers, resulting in a 180° phase difference between two output ports.

The reversely-placed slotline-to-microstrip transitions can be used in the design of out-of-phase power divider. Fig. 14 depicts the transmission line equivalent circuit used in the modelling and synthesis. The transformer at port 3 is reversely placed compared with port 2, which results in 180° phase difference. In this case, the turn ratio value of the slotline-to-microstrip transition at port 3 becomes -n_s in equivalent, which provides a negative sign to reverse the phase. It is noted that the out-of-phase power divider still has the same isolation and matching properties and the same in-band ripple levels with the in-phase one. This is because although the phase response is reversed by the different placement of the slotline-to-microstrip transitions, it does not bring any effect on the magnitude response of the structure.
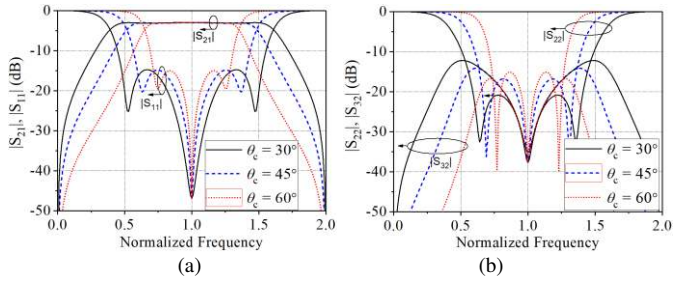
(a)   (b)

Fig. 16. Synthesized S-parameters of the propose power divider when θ_c equals to 30˚, 45˚ and 60˚: (a) |S$_{11}$| and |S$_{21}$|; (b) |S$_{22}$| and |S$_{32}$|.
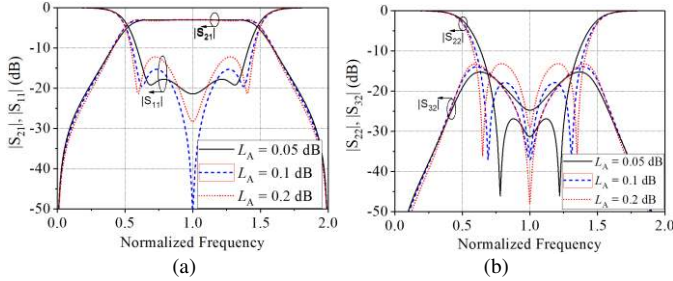

(a)   (b)

Fig. 17. Synthesized S-parameters of the propose power divider when L_A is selected as 0.05 dB, 0.1 dB, and 0.2 dB: (a) |S$_{11}$| and |S$_{21}$|; (b) |S$_{22}$| and |S$_{32}$|.

Fig. 15 shows the layout of the proposed out-of-phase power divider using two different configurations of slotline-to-microstrip transitions. Compared with the in-phase wideband power divider in Fig. 5, the out-of-phase structure adopts exactly the same slotted microstrip T-junction and slotline resonators, while the only difference is the direction of the slotline-to-microstrip transition connected with port 3. In other words, the via-holes and microstrip lines at port 2 and port 3 are placed at the opposite sides of two slotlines in the out-of-phase power divider, which create 180° phase difference between two output signals. In the following part of this section, the in-phase power divider is used for synthesis of the proposed design's magnitude of the frequency response with variable bandwidths and in-band ripple levels.

B. Bandwidth and Constant Magnitude Response

As mentioned before, the proposed power divider is able to achieve flexible fractional bandwidth (FBW) and controllable constant in-band ripple-level at two output ports at the same time. To verify the design approach, several design prototypes are investigated with different fractional bandwidths or in-band ripple levels. Figs. 16(a) and (b) show the scattering parameters of three cases which have equal in-band ripple level and different operating bandwidths. When θ_c is equal to 30˚, 45˚, 60˚ and the in-band ripple level is fixed at 0.1 dB, the coefficient of k_1 and k_2 can be found, and thus the value of z_2 and z_{ss} can be solved. It is observed that to obtain a wider bandwidth, a larger value of z_2 and a smaller value of z_{ss} is required. Meanwhile, when FBW is varied, the matching properties at two output ports and the isolation between two output ports are also affected. When the FBW is extended, the matching and isolation become worse as the maximum reflection and isolation point become larger. When the FBW is narrowed, the matching and isolation become better as the maximum reflection and isolation point become smaller. So for a certain in-band ripple level, the FBW and output matching as
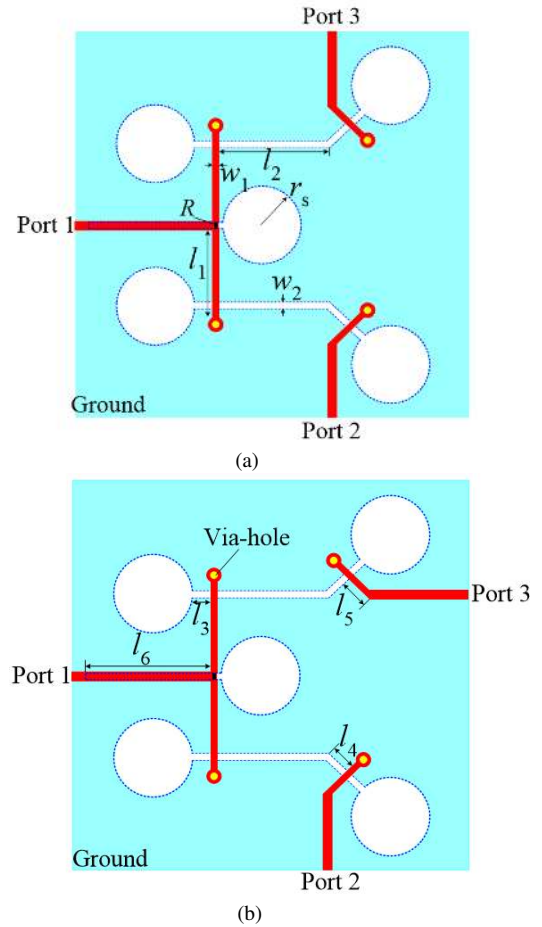

(a)

(b)

Fig. 18. Layout of two designed prototypes with different phase responses: (a) in-phase state; (b) out-of-phase state.

well as isolation are a kind of trade-off and can be balanced as required.

On the other hand, the in-band ripple level can be flexibly controlled without changing the FBW. As a design example, the FBW is selected as 100% as θ_c equates to 45˚. To obtain different in-band levels of 0.05-dB, 0.1-dB and 0.2-dB cases, different values of z_2 and z_{ss} can be solved by putting L_A equal to 0.05, 0.1 and 0.2, respectively. Figs. 17(a) and (b) depict the calculated scattering parameters for the three investigated cases with the same FBW and different in-band ripple-levels. When the ripple level is equal to 0.05 dB, the return loss of S$_{11}$ and S$_{22}$ are quite small at the same time; while when the ripple level increases, the S$_{11}$ and S$_{22}$ will be deteriorated so some extent. In terms of the isolations, when different ripple-levels are selected, the isolation levels for all the cases remain almost the same, which indicates that it is rarely affected by the ripple level and mainly decided by the FBW.

V. EXPERIMENT RESULTS AND DISCUSSIONS

A. Design and Results

Based on the analysis above, two design prototypes with in-phase and out-of-phase responses are fabricated and tested for verification. The design example is aimed at $\theta_c = 45°$, $L_A = 0.1$ dB and 100% operating bandwidth. To that end, the relevant parameters are found to be $Z_1 = 67.2$ Ω, $Z_2 = 55.6$ Ω,
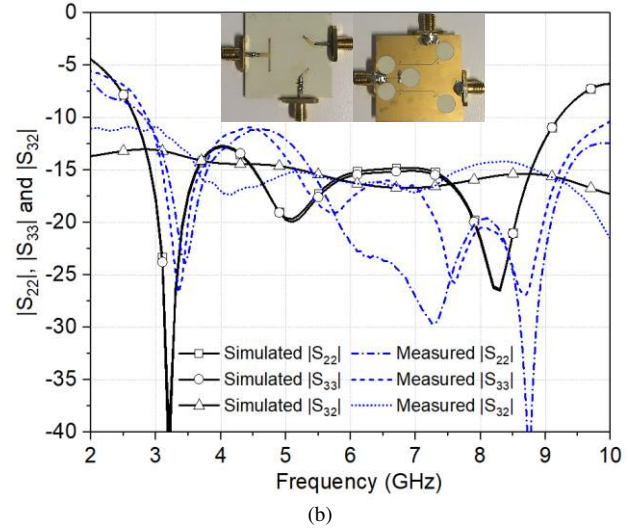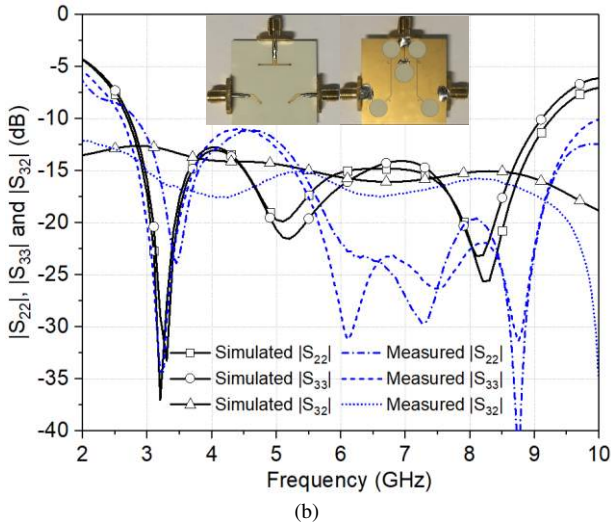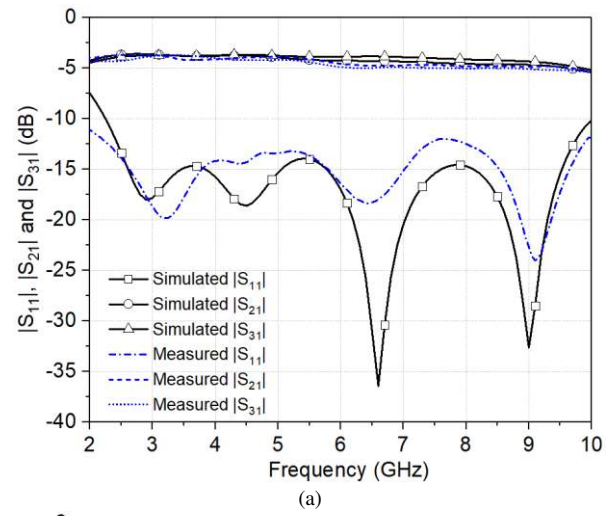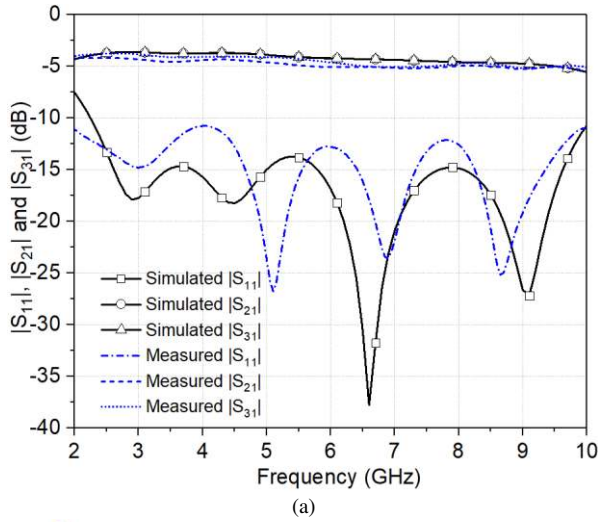
Fig. 19. Simulated and measured results of the in-phase power divider: (a) $|S_{11}|$, $|S_{21}|$ and $|S_{31}|$; (b) $|S_{22}|$, $|S_{33}|$ and $|S_{32}|$.

Fig. 20. Simulated and measured results of the out-of-phase power divider: (a) $|S_{11}|$, $|S_{21}|$ and $|S_{31}|$; (b) $|S_{22}|$, $|S_{33}|$ and $|S_{32}|$.

Fig. 21. Simulated and measured phase difference ($\angle S_{21}$-$\angle S_{31}$) between port 2 and port3 of two prototypes.

and $Z_s = 41.2\ \Omega$. The center frequency is selected as 6 GHz and thus the prospective band range is from 3 GHz to 9 GHz. The substrate employed in this design is Rogers RO4350B with a dielectric constant of 3.48 and thickness of 0.76 mm. The simulation and optimization of the EM model is done using the commercial full-wave simulation software ANSYS Electronics Desktop v.17.2. Figs. 18(a) and (b) show the layout of the prototypes with in-phase and out-of-phase response. Owing to the fabrication tolerance, the impedance of the slotlines is modified in the full-wave simulation based on the synthesized values. Optimization is also done on the overall performance of the device. The final dimensions shown in Fig. 14 are listed as: $l_1 = 5.7$, $l_2 = 14.5$, $l_3 = 1.6$, $l_4 = 1.8$, , $l_5 = 5.7$, $l_6 = 17.2$, $w_1 = 0.53$, $w_2 = 0.2$, $r_s = 4.2$, all in mm. A chip resistor R with 100 Ω is embedded across the slot on the ground in both structures. The overall size of each circuit is around 32.4 mm × 25.9 mm.

The fabricated prototypes are finally tested using vector network analyzer. The simulated and measured results are shown in Figs. 19-21. For the in-phase case, Fig. 19 shows the measured and simulated performance. It is observed from Fig. 19(a) that the measured return loss is below -11.2 dB, compared

with the simulated -13.5 dB from 2.5 GHz to 10 GHz. The measured insertion loss is around 0.8 to 2 dB, which is very close to the simulated one. Fig. 19(b) shows the simulated and tested isolation and matching properties at output ports. Within the band range, the isolation is below -15 dB across the whole

TABLE I
COMPARISON BETWEEN THE PROPOSED DESIGNS WITH OTHER WORKS

Ref.	Type	RL (dB)	IL (dB)	Isolation (dB)	FBW	Equal-ripple	Microstrip compatibility
[1]	In-phase	-10	0.4-1.2	-10	97%	No	Yes
[3]	In-phase	-10	1-2	-10	105%	No	No
[4]	In-phase	-14	1-3	-12	109%	No	No
[5]	In-phase	-13	0.6	-10	109%	No	Yes
[6]	In-phase	-10	N.P.	-14	54%	No	Yes
[18]	In-phase	-15	0.66	-15	104.5%	No	Yes
[19]	Out-of-phase	-10	0.5	-10	105%	No	No
[20]	Out-of-phase	-10	2.5	-9	40%	No	No
[21]	Out-of-phase	-10	0.5	-8	109%	No	Yes
[23]	Out-of-phase	-10	N.P.	-16	66%	No	Yes
This	**In-phase**	**-11**	**0.8-2**	**-13**	**110%**	**Yes**	**Yes**
work	**Out-of-phase**	**-12**	**1-2.2**	**-15**	**110%**	**Yes**	**Yes**

RL: return loss; IL: insertion loss; FBW: fractional bandwidth; N.P.: not provided.
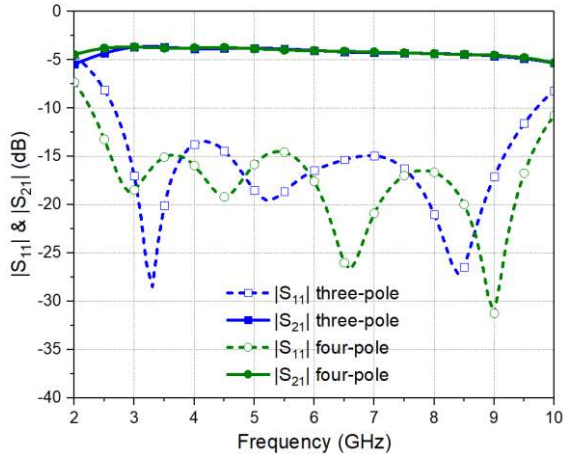

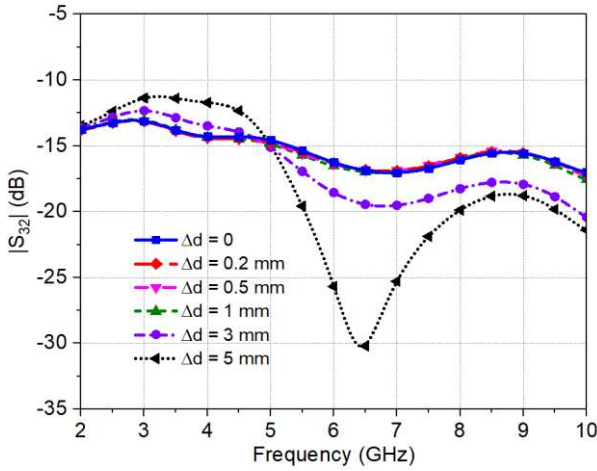Fig. 22. Comparison of $|S_{21}|$ between the three-pole and four-pour design.

Fig. 23. Effect on $|S_{32}|$ when the resistor is located at different positions.

band range. Besides, excellent matching properties can be observed as the measured return loss at output ports is all less than -11.5 dB. For the out-of-phase design, the simulated and measured results are displayed in Fig. 20. Less than -12 dB return loss at the input port is achieved from the measurement, compared with -13.8 dB from simulation. The insertion loss is around 1.0 to 2.2 dB, which is close to the simulated one. Good matching and isolation properties are obtained as well: the return loss at output port is less than -11 dB from 2.8 GHz to

more than 10 GHz, while the isolation is below -13 dB across the same band range.

Fig. 21 shows the simulated and tested phase difference between port 2 and port 3 ($\angle S_{21} - \angle S_{31}$) of both prototypes. The measured phase difference is found to be less than ±2.0° and ±2.4° degree, compared with ±0.2° and ±0.8° from simulation, respectively. This demonstrates the proposed power dividers have excellent linearity of phase across an extremely wide operating band range. Considering the overall performance of two prototypes, around 109.7% bandwidth (from 2.8 GHz to 9.6 GHz) can be claimed from the tested results of both designs. The photos of two fabricated prototypes have been included in Figs. 19(b) and 20(b). Since the focus of this work is mainly on the bandwidth and in-band magnitude performance of the design, the out-of-band result is not displayed. It is notable that due to the radiation of transmitted signals at high frequencies (from 6 GHz and above), the insertion loss is slightly increased, which can be observed from the tested results of both prototypes. This extra loss can be prevented by adding a metallic shield enclosing the board, which is important when the circuit is integrated and utilized in systems.

B. Discussions

To demonstrate the advantages of this work, a comparison is given in TABLE I. From TABLE I one can find that, this work realized ultra-wide operating bandwidth with excellent isolation performance. The proposed design is the first work to realize equal and constant in-band ripple for the magnitude response using multi-mode resonators. Besides, it is also the first work to realize both in-phase and out-of-phase responses with ultra-wide bandwidth using a simple structure.

As mentioned earlier, due to the limitation of fabrication tolerance, the smallest realizable value of the impedance is 64 Ω using the adopted substrate. Accordingly, the related values for the model is modified in the full-wave simulation. Using very narrow width of slotlines ($w_2 = 0.05$ mm), a three-pole response can be obtained. In the current design, the width of w_2 is selected as 0.2 mm, and thus the second transmission pole will be split into two, resulting in a four-pole response within the operating band. The comparison of $|S_{21}|$ between the three-pole and four-pole responses is shown in Fig.

22. It is seen that the return loss levels are almost the same in two cases, while the four-pole design has a slightly wide bandwidth than the three-pole case. To maintain a constant and equal in-band ripple magnitude response as well as excellent isolation performance within the passband, the whole structure is optimized as the final step in the design procedure.

Another issue to be noted is the isolation performance of the design, which is also an advantage of this work. The design can realize excellent isolation across ultra-wide band range, which is largely attributed to the loaded resistor on the slotted ground. The resistor should be placed at the connecting point of the circular slot and the slotline stub. To investigate the effect of the resistor location on the isolation, multiple simulations have been done as shown in Fig. 23. Here Δd refers to the distance that the resistor is moved away from the original place along the slotline on the backside of the feed. It is seen that when Δd is less than 1 mm, $|S_{32}|$ remains exactly the same. When Δd is increased to 3 mm or even 5 mm, the isolation becomes less balanced at lower and higher frequencies. In all simulations, the highest response level in $|S_{32}|$ appears at 3.5 GHz and 8.5 GHz, which are in line with the resonant frequencies of the power divider. This phenomenon can also be observed in the synthesis, which demonstrates that the proposed design can achieve high isolation across the entire band.

VI. Conclusion

A planar wideband power divider has been presented and verified via theoretical analysis and experiments. Microstrip-to-slotline transitions and slotline resonators have been used to achieve equal in-band ripple response. To investigate the relation between the structure and the achievable FBW and in-band ripple-level, the proposed power divider has been synthesized using its transmission line equivalent circuit. Based on the analysis, the structure can achieve constant in-band magnitude response and flexible bandwidth by controlling the dimensions of microstrip-to-slotline transitions and the slotline resonator. Based on proposed design approach, a wideband power divider has been built, simulated and optimized via full-wave simulations. The experimental results have demonstrated that excellent matching and isolation and wide operating bandwidth can be obtained. In-phase and out-of-phase responses are achieved for wideband applications using one structure. A constant in-band magnitude response and minimal insertion loss imbalance have been obtained, which is highly desired in wireless communications systems.

References

[1] S. W. Wong and L. Zhu, "Ultra-wideband power divider with good in-band splitting and isolation performances," *IEEE Microw. Wireless Compon. Lett.,* vol. 18, no. 8, pp. 518-520, Aug. 2008.

[2] S. W. Wong and L. Zhu, "Ultra-wideband power dividers with good isolation and improved sharp roll-off skirt," *IET Microw. Antennas Propag.*, vol. 3, no. 8, pp. 1157–1163, Dec. 2009.

[3] K. Song and Q. Xue, "Novel ultra-wideband (UWB) multilayer slotline power divider with bandpass response," *IEEE Microw. Wireless Compon. Lett.*, vol. 20, no. 1, pp. 13–15, Jan. 2010.

[4] A. M. Abbosh, "Design of ultra-wideband three-way arbitrary power dividers," *IEEE Trans. Microw. Theory Techn.*, vol. 56, no. 1, pp. 194–201, Jan. 2008.

[5] L. Guo, A. Abbosh, and H. Zhu, "Ultra-wideband in-phase power divider using stepped-impedance three-line coupled structure and microstrip-to-slotline transitions," *Electron. Lett.*, vol. 50, no. 5, pp. 383–384, Feb. 2014.

[6] D. Chen, L. Zhu and C. Cheng, "Dual-Resonant-Mode (DRM) Impedance Transformer and Its Application to Wideband 3 dB Power Divider", *IEEE Microwave and Wireless Components Letters*, vol. 23, no. 9, pp. 471-473, 2013.

[7] H. Oraizi and A.-R. sharifi, "Optimum design of asymmetrical multisection two-way power dividers with arbitrary power division and impedance matching," *IEEE Trans. Microw. Theory Tech.*, vol. 59, no. 6, pp. 1478–1490, Jun. 2011.

[8] F. Lin, Q.-X. Chu, Z. Gong, and Z. Lin, "Compact broadband Gysel power divider with arbitrary power dividing ratio using microstrip/slotline phase inverter," *IEEE Trans. Microw. Theory Techn.*, vol. 60, no. 5, pp. 1226–1234, May 2012.

[9] S. S. Gao, S. Sun, and S. Q. Xiao, "A novel wideband bandpass power divider with harmonic-suppressed ring resonator," *IEEE Microw. Wireless Compon. Lett.*, vol. 23, no. 3, pp. 119–121, Mar. 2013.

[10] X. Y. Zhang, K.-X. Wang, and B.-J. Hu, "Compact filtering power divider with enhanced second-harmonic suppression," *IEEE Microw. Wireless Compon. Lett.*, vol. 23, no. 9, pp. 483–485, Sep. 2013.

[11] Y. C. Li, Q. Xue, and X. Y. Zhang, "Single- and dual-band power dividers integrated with bandpass filters," *IEEE Trans. Microw. Theory Techn.*, vol. 61, no. 1, pp. 69–76, Jan. 2013.

[12] C. -F. Chen, T. -Y. Huang, T. -M. Shen, and R. -B. Wu, "Design of miniaturized filtering power dividers for system-in-a-package," *IEEE Trans. Compon., Packag., Manuf. Technol.*, vol. 3, no. 10, pp. 1663–1672, Oct. 2013.

[13] K. Song, Y. Mo, and Y. Fan, "Wideband four-way filtering-response power divider with improved output isolation based on coupled lines," *IEEE Microw. Wireless Compon. Lett.*, vol. 24, no. 10, pp. 674–676, Oct. 2014.

[14] H. Zhu, A. Abbosh, and L. Guo, "Wideband four-way filtering power divider with sharp selectivity and wide stopband using looped coupledline structures," *IEEE Microw. Wireless Compon. Lett.*, vol. 26, no. 6, pp. 413–415, Jun. 2016.

[15] Q. Li, Y. Zhang, C. M. Wu, "High-selectivity and miniaturized filtering wilkinson power dividers integrated with multimode," *IEEE Trans. Compon., Packag., Manuf. Technol.*, vol. 7, no. 12, pp. 1990–1997, Dec. 2017.

[16] H. Zhu, and A. M. Abbosh, "Compact ultra-wideband in-phase power divider using three-line coupled structure," in *Proc. Antennas Propag. Soc. Int. Symp. (APSURSI)*, Jul. 2014, pp. 820–821.

[17] C.-W. Tang and Z.-Q. Hsieh, "Design of a planar dual-band power divider with arbitrary power division and a wide isolated frequency band*,*" *IEEE Trans. Microw. Theory Techn.*, vol. 64, no. 2, pp. 486–492, Feb. 2016.

[18] C.-W. Tang and J.-T. Chen, "A design of 3-dB wideband microstrip power divider with an ultra-wide isolated frequency band," *IEEE Trans. Microw. Theory Techn.*, vol. 64, no. 6, pp. 1806–1811, Jun. 2016.

[19] J.-X. Chen, C. H. K. Chin, K. W. Lau, and Q. Xue, "180° out-of-phase power divider based on double-sided parallel striplines," *Electron Lett.*, vol. 42, no. 21, pp. 1229–1230, Oct. 2006.

[20] K. Eccleston, "Folded substrate-integrated waveguide out-of-phase power divider," in *Proc. Asia-Pacific Microw. Conf.*, Dec. 2010, pp. 1260–1263.

[21] M. E. Bialkowski and A. M. Abbosh, "Design of a compact UWB out-of-phase power divider," *IEEE Microw. Wireless Compon. Lett.*, vol. 17, no. 4, pp. 289–291, Apr. 2007.

[22] U. T. Ahmed and A. Abbosh, "Wideband out-of-phase power divider using tightly coupled lines and microstrip to slotline transitions", *Electron. Lett.*, vol. 52, no. 2, pp. 126-128, 2016.

[23] A. M. Abbosh, "Planar out-of-phase power divider/combiner for wideband high power microwave applications," *IEEE Trans. Compon. Packag. Manuf. Technol.*, vol. 4, no. 3, pp. 465–471, Mar. 2014.

[24] R. Li, S. Sun, and L. Zhu, "Synthesis design of ultra-wideband bandpass filters with composite series and shunt stubs," *IEEE Trans. Microw. Theory Techn.*, vol. 57, no. 3, pp. 684–692, Mar. 2009.

[25] X. Guo, L. Zhu, J. Wang, and W. Wu, "Wideband microstrip-to-microstrip vertical transitions via multiresonant modes in a slotline

resonator," *IEEE Trans. Microw. Theory Techn*., vol. 63, no. 6, pp. 1902–1909, Jun. 2015.

[26] L. Yang, L. Zhu, W. W. Choi, and K. –W Tam, "Analysis and design of wideband microstrip-to-microstrip equal ripple vertical transitions and their application to bandpass filters," *IEEE Trans. Microw. Theory Techn*., vol. 65, no. 8, pp. 2866–2877, Aug. 2017.

[27] I. Sakagami, K. Sagaguti, M. Fujii, M. Tahara, and Y. Hao, "On a lumped element three-branch 3-dB coupler with Butterworth and Chebyshev characteristic," in *IEEE Int. Midwest Circuits Syst. Symp*., 2004, pp. III-21–III-24.

[28] H. J. Wei, C. C. Meng, and S. W. Yu, "A Chebyshev-response step impedance phase-inverter rat-race coupler directly on lossy silicon substrate and its Gilbert mixer application," *IEEE Trans. Microw. Theory Tech.*, vol. 59, no. 4, pp. 882–893, Apr. 2011.

[29] L. -P. Feng, and L. Zhu, "Wideband filtering balun on a novel hybrid multimode resonator with the functionality of vertical transition," *IEEE Trans. Compon., Packag., Manuf. Technol.*, vol. 7, no. 8, pp. 1324–1330, Aug. 2017.

[30] Y. -P. Lyu, L. Zhu, Q. -S. Wu, and C.-H. Cheng, "Proposal and synthesis design of wideband phase shifters on multimode resonator," *IEEE Trans. Microw. Theory Techn*., vol. 64, no. 12, pp. 4211–4221, Dec. 2016.

[31] Q. S. Wu, and L. Zhu, "Short-ended coupled-line impedance transformers with ultrahigh transforming ratio and bandpass selectivity suitable for large load impedances," *IEEE Transactions on Components, Packaging and Manufacturing Technology*, vol. 6, no. 5, pp. 767–774, 2016.

[32] Q. S. Wu, and L. Zhu, "Wideband impedance transformers on parallel coupled and multisection microstrip lines: Synthesis design and implementation," *IEEE Trans. Compon., Packag., Manuf. Technol*., vol. 6, no. 12, pp. 1873–1880, Dec. 2016.

[33] M. Bialkowski and Y. Wang, "Wideband microstrip 180° hybrid utilizing ground slots," *IEEE Microw. Wireless Compon. Lett.*, vol. 20, no. 9, pp. 495–497, Sep. 2010.

[34] Y. Wang, M. E. Bialkowski, and A. M. Abbosh, "Double microstripslot transitions for broadband ±90 degrees microstrip phase shifters," *IEEE Microw. Wireless Compon. Lett.,* vol. 22, no. 2, pp. 58–60, Feb. 2012.

[35] B. Henin and A. Abbosh, "Wideband hybrid using three-line coupled structure and microstrip-slot transitions," *IEEE Microw. Wireless Compon. Lett*., vol. 23, no. 7, pp. 335–337, Jul. 2013.

[36] K. C. Gupta, R. Garg, I. Bahl, and P. Bhartia, *Microstrip Lines and Slotlines*, 2nd ed. Norwood, MA: Artech House, 1996, pp. 108–109.

[37] B. Schuppert, "CAD of nonlinear microwave devices: Development of a balanced mixer having more than 3 octaves bandwidth," in *Proc. 15th Europeun Microwave Conf.,* 1985, pp. 527-532.

[38] B. Schuppert, "Analysis and design of microwave balanced mixers," *IEEE Trans. Microwave Theory Tech.,* vol. MTT-34, pp. 120-128, Jan. 1986.

[39] J. Chramiec, "Reactances of slotline short and open circuits on alumina substrate," IEEE Trans. Microwave Theory Tech., vol. 37, pp. 1638-1641, 1989.

[40] B. Schiippert, "Microstrip/slotline transitions: modeling and experimental investigation," *IEEE Trans. Microwave Theory Tech*., vol. 36, no. 8, pp. 1272-1282, Aug. 1988.

[41] J. -C. Kao, Z. -M. Tsai, K. -Y. Lin, and H. Wang, "A modified Wilkinson power divider with isolation bandwidth improvement," *IEEE Trans. Microw. Theory Techn.*, vol. 60, no. 9, pp. 2768–2780, Sep. 2012.

[42] W. Choe and J. Jeong, "Compact modified Wilkinson power divider with physical output port isolation," *IEEE Microw. Wireless Compon. Lett*., vol. 24, no. 12, pp. 845–847, Dec. 2014.

[43] I. Sakagami, X. Wang, K. Takahashi, and S. Okamura, "Generalized two-way two-section dual-band Wilkinson power divider with two absorption resistors and its miniaturization," *IEEE Trans. Microw. Theory Tech.*, vol. 59, no. 11, pp. 2833–2847, Nov. 2011.

[44] X. Wang, I. Sakagami, K. Takahashi, and S. Okamura, "A generalized dual-band Wilkinson power divider with parallel *L*, *C*, and *R* components," *IEEE Trans. Microw. Theory Tech*., vol. 60, no. 4, pp. 952–964, Apr. 2012.

[45] X. Wang, I. Sakagami, A. Mase, and M. Ichimura, "Wilkinson power divider with complex isolation component and its miniaturization," *IEEE Trans. Microw. Theory Tech*., vol. 62, no. 3, pp. 422-430, Mar. 2014.

[46] F. C. de Ronde, "A new class of microstrip directional couplers," in *IEEE MTT-S Int. Microwave Symp. Dig.*, 1970, pp. 184-186.